The Journal of Chemical Physics

Reducing bias in the analysis of solution-state NMR data with dynamics detectors

Cite as: J. Chem. Phys. **151**, 034102 (2019); https://doi.org/10.1063/1.5111081
Submitted: 23 May 2019 . Accepted: 09 June 2019 . Published Online: 15 July 2019

Albert A. Smith, Matthias Ernst, Beat H. Meier, and Fabien Ferrage

The Journal of Chemical Physics ARTICLE scitation.org/journal/jcp

Reducing bias in the analysis of solution-state NMR data with dynamics detectors

Cite as: J. Chem. Phys. 151, 034102 (2019); doi: 10.1063/1.5111081
Submitted: 23 May 2019 • Accepted: 9 June 2019 •
Published Online: 15 July 2019

Albert A. Smith,[1,a] Matthias Ernst,[1,b] Beat H. Meier,[1,c] and Fabien Ferrage[2,d]

AFFILIATIONS

[1] ETH Zurich, Physical Chemistry, Vladimir-Prelog-Weg 2, 8093 Zurich, Switzerland

[2] Laboratoire des biomolécules, LBM, Département de chimie, École normale supérieure, PSL University, Sorbonne Université, CNRS, 75005 Paris, France

[a] **Present address:** Universität Leipzig, Insitut für Medizinische Physik und Biophysik, Härtelstraße 16-18, 04107 Leipzig, Germany.
[b] maer@ethz.ch
[c] beme@ethz.ch
[d] Fabien.Ferrage@ens.fr

ABSTRACT

Nuclear magnetic resonance (NMR) is sensitive to dynamics on a wide range of correlation times. Recently, we have shown that analysis of relaxation rates via fitting to a correlation function with a small number of exponential terms could yield a biased characterization of molecular motion in solid-state NMR due to limited sensitivity of experimental data to certain ranges of correlation times. We introduced an alternative approach based on "detectors" in solid-state NMR, for which detector responses characterize motion for a range of correlation times and reduce potential bias resulting from the use of simple models for the motional correlation functions. Here, we show that similar bias can occur in the analysis of solution-state NMR relaxation data. We have thus adapted the detector approach to solution-state NMR, specifically separating overall tumbling motion from internal motions and accounting for contributions of chemical exchange to transverse relaxation. We demonstrate that internal protein motions can be described with detectors when the overall motion and the internal motions are statistically independent. We illustrate the detector analysis on ubiquitin with typical relaxation data sets recorded at a single high magnetic field or at multiple high magnetic fields and compare with results of model-free analysis. We also compare our methodology to LeMaster's method of dynamics analysis.

I. INTRODUCTION

Nuclear magnetic resonance (NMR) is a powerful analytical tool for the investigation of the structure and dynamics of biomolecules with atomic resolution. Biomolecular dynamics of picoseconds to nanoseconds are most often characterized by NMR relaxation.[1,2] The analysis of NMR relaxation-rate constants may be based on models of internal motion,[3–5] but most investigations of picosecond-nanosecond motions rely on an approach that leaves aside assumptions about the physical nature of the motions and is thus called model-free.[6–9]

Relaxation-rate constants are linked to dynamic processes through the spectral-density function, which is the Fourier transform of the correlation function.[10,11] For typical dipole-dipole interactions, this is the correlation function for internuclear vectors, which provides direct access to molecular motions. The spectral density function is probed at the eigenfrequencies of the spin system under investigation (e.g., near the Larmor frequencies), and one then assumes the correlation function of motion to consist of one or several decaying exponential terms and attempts to fit a correlation time and amplitude for each term. When using one exponential term to describe internal motion of a molecule tumbling in solution, this is referred to as the model-free approach,[9] whereas the extended model-free approach may have two or more terms to model the internal motion.[6] "Model-free" is sometimes also applied to solid-state relaxation analysis, although the original usage referred only to a solution-state method. In solution- and solid-state NMR, the limited sampling of the spectral-density function restricts the number

of terms that may be fitted, which can be a source of bias. We have recently investigated the effect of the limited information in ensembles of relaxation rates in solid-state NMR and demonstrated that analysis with inappropriate models could result, in the worst case, in parameters of dynamics whose true values are significantly outside the confidence interval of the fitted correlation times and order parameters.[12,13]

Here, we investigate whether dynamics analysis with several internal motions in solution-state NMR is likely to suffer from similar distortions as can occur in solid-state NMR. This can be easily tested by calculating rate constants for a correlation function with several exponential terms and then testing the fit performance when a simpler, model correlation function is used to fit the calculated rate constants. We calculated a set of longitudinal, R_1, and transverse, R_2, rate constants, as well as the dipolar cross-relaxation rate constant, σ_{NH}, for a molecule tumbling isotropically in solution, with a tri-exponential correlation function for internal motions [amplitudes, $(1 - S^2)A_k$, and correlation times, τ_c, in Fig. 1(a)]. Such a tri-exponential correlation function of an H–N bond can result, for example, from a combination of very fast, librational motions (here assumed at 1 ps), motion of the peptide plane (320 ps), and a slower loop motion involving correlated motion of several residues (3.2 ns). Note that, in reality, we could expect such dynamics to result in a distribution of correlation times for each motion, but for simplicity we assume just three discrete correlate times. The calculated relaxation data set was fitted with a bi-exponential correlation function for internal motions. We find excellent reproduction of the rate constants in Fig. 1(b); however, the fitted correlation times and amplitudes of the exponential terms are far from the input amplitudes and correlation times. This result indicates that such a large set of relaxation rates fails to distinguish between the simple model used in the analysis and the true, more complex model of the internal motion. Clearly, the subsequent mechanistic interpretation of results of the analysis of relaxation rates with a model that is too simple would lead to an erroneous picture of dynamics (further examples are shown in Fig. S6).

A number of approaches already address these shortcomings, but each has limitations. Spectral-density mapping, for example, determines the values of the spectral density function only at a few frequencies that determine measured relaxation rates.[14–16] This requires minimal assumptions about the complexity of motion and so limits biasing. While the original method uses R_1, σ_{NH}, and R_2 at a single field, it is possible to exploit near-coincidence of frequencies in multifield data sets to obtain further information.[17,18] However, because it does not retrieve the correlation times or amplitudes of motional modes, the interpretation of spectral density mapping is mostly qualitative[19] and does not separate contributions from internal and overall (tumbling) motion. Other attempts have been made to recover information about the correlation times of motions that lead to relaxation with minimal bias. For instance, the interpretation of motions by projection on an array of correlation times (IMPACT) determines the distribution of correlation times through a simple regularization method and was applied to the analysis of relaxation in disordered proteins.[20] Similar to spectral density mapping, IMPACT does not remove the influence of tumbling. Finally, LeMaster developed an approach in which R_1, σ_{NH}, and R_2 are fitted, using fixed correlation times.[21] In this approach, LeMaster was successful in separating internal motion from tumbling, but his approach is limited to analyzing data sets recorded at a single magnetic field.

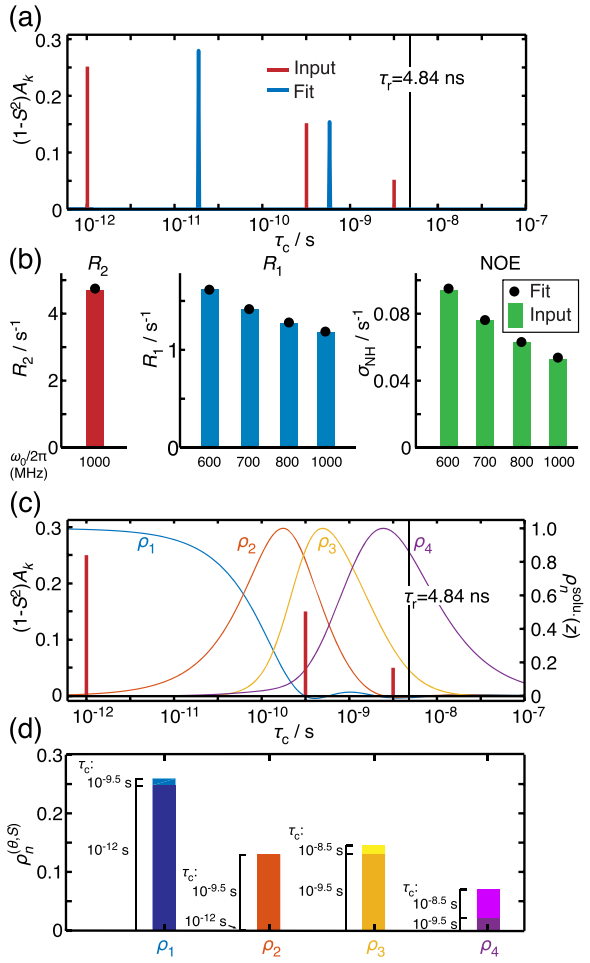

FIG. 1. Problematic fit behavior in solution-state NMR: Synthetic data for ^{15}N R_2 at 1000 MHz and ^{15}N R_1 and ^{1}H–^{15}N σ_{NH} (measured from nuclear Overhauser effects, NOE), at 600, 700, 800, and 1000 MHz for H–N backbone dynamics in solution-state NMR, for a correlation function with three correlation times. The input correlation function is shown as a function of the correlation time in (a) (red lines), with amplitudes of motion shown on the *y*-axis for a protein tumbling with τ_r = 4.84 ns. The resulting rate constants [(b), bars] are then fitted to a model correlation function having only two internal correlation times. The fitted amplitudes and correlation times are shown in (a) (blue lines), and the calculated rate constants are shown in (b) (black circles). Although a close-to-perfect fit of the rate constants is obtained, the resulting amplitudes and correlation times are far away from the input motion. Note that R_2 rate constants obtained at different fields contain very little independent information so that we only show a single rate constant here (multiple R_2 rate constants could also easily be fit). (c) plots the sensitivities of a set of four detectors that are calculated using this data set. The amplitudes and correlation times of the input correlation function are replotted (red) to show the overlap of the motion and the sensitivities. (d) shows the detector responses, which give the overlap of the sensitivities with amplitudes and correlation times. Bars are separated into sections, indicating how each motion contributes to the total detector responses.

To address distortions from using an over-simplified model of the correlation function in solid-state NMR (sometimes also referred to as model-free), we have recently introduced an approach based on dynamics detectors, which are linear combinations of relaxation-rate constants, where the linear combinations are optimized to yield information about different ranges of correlation times.[12,13] A set of detectors is built for each relaxation data set, based on the relaxation-rate constants measured, for example, at different magnetic fields. Then, resulting detector sensitivities indicate what range of correlation times the set of experiments is sensitive to and further indicate how well one may resolve different ranges of correlation times. Experimental data analysis then quantifies how much motion is in the sensitive range of each detector. More precisely, detectors yield the overlap of a sensitivity function and a distribution of correlation times of motion. For example, in Fig. 1(c), four detector sensitivities are shown, where the overlap of these sensitivities with the three correlation times and amplitudes in Figs. 1(a)/1(c) results in the detector responses shown in Fig. 1(d). This approach provides quantitative information about the correlation times and amplitudes of motions with minimal assumptions about the motions.[13] Detector sensitivities clearly indicate the range of correlation times that is probed by the set of experiments and the resolution at which correlation times can be defined. By contrast, modeling the correlation function with a few decaying exponentials results in correlation times that are a function of the internal motion and of the choice of experiments.[12] As with spectral-density mapping and the IMPACT approach, detectors as previously described do not allow separation of tumbling and internal motion [Figs. 1(c)/1(d) shows detectors that *do* separate tumbling and internal motion, using the methodology that we will present below].

Detectors characterize the overlap of the detector sensitivities with the distribution of motion so that the resulting dynamics description may seem rather imprecise as compared to the seemingly well-defined correlation times and amplitudes (order parameters) resulting from modeling the correlation function as a few decaying exponentials. However, as we have shown in Fig. 1 and previously,[12] these correlation times can represent poorly defined averages of the "true" correlation times of multiple motions. To better understand the complications brought about by this averaging process, we consider another example. We continue with the assumption of a motional model defined by three correlation times, now fixed at correlation times for fast motion, $\tau_{f,in}$ = 1 ps; for intermediate motion, $\tau_{i,in}$ = 300 ps; and for slow motion, $\tau_{s,in}$ = 3 ns. The order parameters for the two motions with shorter correlation times are also fixed at $(1 - S^2)A_{f,in} = 0.25$, $(1 - S^2)A_{i,in} = 0.15$ [where $(1 - S^2)A_{f,in} = (1 - S^2_{f,in})$, $(1 - S^2)A_{i,in} = S^2_{f,in}(1 - S^2_{i,in})$]. The amount of slow internal motion, corresponding to the correlation time $\tau_{s,in}$ = 3 ns, is allowed to vary from $(1 - S^2)A_{s,in} = 0$ to $(1 - S^2)A_{s,in} = 0.21$ [$(1 - S^2)A_{s,in} = S^2_{f,in}S^2_{i,in}(1 - S^2_{s,in})$]. Relaxation-rate constants resulting from this correlation function are then fitted using a bi-exponential correlation function (using the same set of simulated relaxation data as in Fig. 1), with results in Fig. 2(a).

When $(1-S^2)A_{s,in} = 0$, the input motion has only two terms, so the parameters of the fitted model match the input model, yielding a perfect fit. When $(1 - S^2)A_{s,in}$ increases, the fitted $(1 - S^2)A_{s,fit}$ also increases since it now contains contributions from both $(1-S^2)A_{s,in}$ and $(1 - S^2)A_{i,in}$. Correspondingly, $\tau_{s,fit}$ also increases from contributions from the slow motion. However, we also see that there is about a 15% increase in $(1-S^2)A_{f,fit}$ and more than an order of magnitude change in $\tau_{f,fit}$. Then, we see that a very slow motion (here

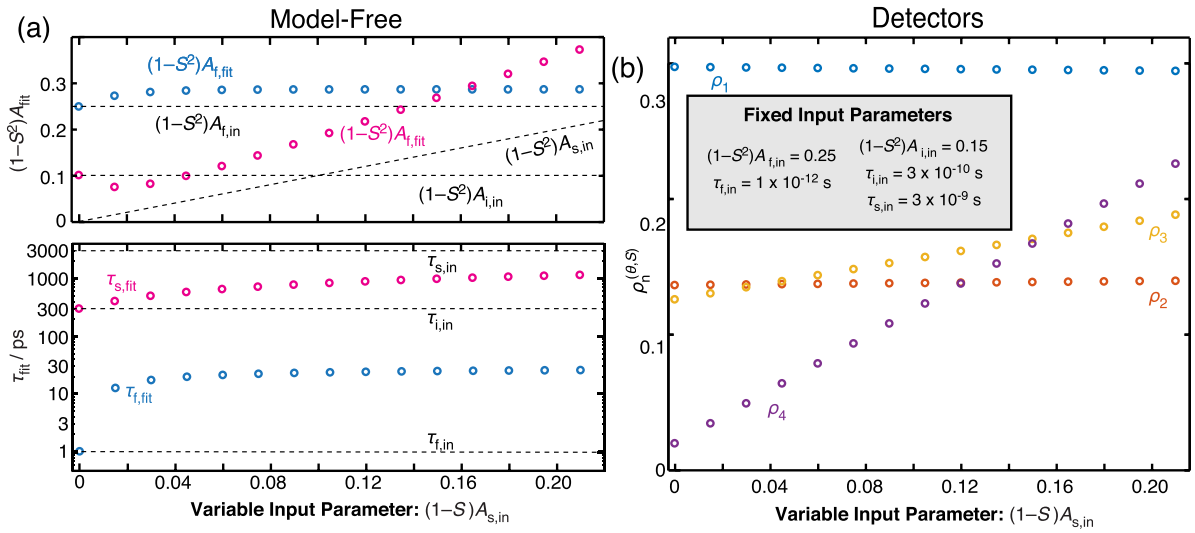

FIG. 2. Model-free and detector behavior as a function of motional amplitude. We assume a model with three correlation times, with all parameters but the order parameter of the slowest motion fixed [$(1 - S^2)A_{f,in} = 0.25$, $\tau_{f,in} = 1 \times 10^{-12}$ s, $(1 - S^2)A_{i,in} = 0.15$, $\tau_{i,in} = 3 \times 10^{-10}$ s, $\tau_{s,in} = 3 \times 10^{-9}$ s]. (a) shows fitted amplitudes (top) and correlation times (bottom) as a function of the amplitude of the input slow motion, $(1 - S^2)A_{s,in}$, resulting from fitting rate constants using a bi-exponential correlation function (same experiments as in Fig. 1). Black dashed lines show the input parameters. (b) shows detector responses for the same motions, using the detector sensitivities given in Fig. 1(c).

3 ns) can influence a fitted parameter that corresponds to motion two orders of magnitude faster (with $\tau_{f,fit} \leq 25$ ps). This relayed influence of a slow motion on fast-motional parameters can potentially convolute the interpretation of model-free results.

The effect of the change in amplitude $(1-S^2)A_{s,in}$ on the detector analysis is more regular [Fig. 2(b)]. Increasing the amplitude results in a strong increase in $\rho_4^{(\theta,S)}$, which is expected since the maximum of the ρ_4 detector sensitivity is close to 3 ns, and a smaller increase in $\rho_3^{(\theta,S)}$ since the ρ_3 sensitivity is nonzero at 3 ns [Fig. 1(c)]. Critically, $\rho_1^{(\theta,S)}$ and $\rho_2^{(\theta,S)}$ are not visibly influenced by the slow motion since they are only sensitive to short correlation times. An increase in the amplitude in a motion results simply in the increase in detector responses sensitive to the correlation time of that motion, with no effects on the other detectors.

Neither model-free analysis nor detectors allow us to recover a complete description of the original motion. On the other hand, given the original motion, we may directly determine detector responses (which will be precisely defined below), but we may not easily determine the model-free parameters except for special cases.[9,22] While both methods leave ambiguity in describing the original motion, detector sensitivities give a clear indication as to where these ambiguities are, via detector sensitivities. These advantages are particularly important when comparing NMR analyses to other methods, such as molecular dynamics simulations.[23]

Here, we present a modified detector framework adapted to the analysis of solution-state relaxation, where the influence of the overall rotational diffusion (tumbling) of a macromolecule on the detector responses is removed. We have also expanded the DIFRATE software with updated methodology[24] and analyzed typical data sets recorded at one to three static magnetic fields. We compare the results to analyses of data using the extended model-free approach and find that we obtain a more stable and easier to interpret description of the internal dynamics. We also compare our approach to that of LeMaster for the analysis of relaxation rate constants recorded at a single magnetic field; the methods yield very similar behavior so that LeMaster's approach may be considered as a special case of the detector approach.[21]

II. THEORY

A. Background

In NMR dynamics, one often assumes that the internal motion may be described by a correlation function, $C_I(t)$, consisting of one or more exponential terms[9] so that one can write

$$C_I(t) = S^2 + (1-S^2)\sum_k A_k \exp(-t/\tau_k). \tag{1}$$

Then, $(1-S^2)$ is related to the total amplitude of internal motion, and A_k give contributions from individual internal motions at effective correlation times τ_k (A_k sum to 1). In the case of solution-state NMR, we usually assume separability (statistical independence)[25] of internal and overall motions leading, for isotropic tumbling, to a total correlation function of

$$\begin{aligned} C(t) &= C_O(t)C_I(t), \\ C_O(t) &= \frac{1}{5}\exp(-t/\tau_r), \end{aligned} \tag{2}$$

where $C_O(t)$ is the correlation function of the overall motion, and τ_r is the corresponding rotational correlation time.[9]

From $C(t)$, we obtain the spectral-density function

$$J(\omega) = 2\int_0^\infty C(t)\cos(\omega t)dt \tag{3}$$

and subsequently calculate various relaxation-rate constants. In this study, we will primarily concentrate on R_1, R_2, and the dipolar cross-relaxation rate constant, σ_{IS} [measured through nuclear Overhauser effects (NOE)],

$$R_1 = \left(\frac{\delta_{IS}}{4}\right)^2 (J(\omega_I-\omega_S) + 3J(\omega_I) + 6J(\omega_I+\omega_S)) + \frac{1}{3}(\omega_I\Delta\sigma_I)^2 J(\omega_I), \tag{4}$$

$$R_2 = \frac{1}{2}R_1 + \left(\frac{\delta^{IS}}{4}\right)(3J(\omega_S) + 2J(0)) + \frac{2}{9}(\omega_I\Delta\sigma_I)^2 J(0), \tag{5}$$

$$\sigma_{IS} = \left(\frac{\delta_{IS}}{4}\right)^2 (-J(\omega_I-\omega_S) + 6J(\omega_I+\omega_S)). \tag{6}$$

Here, δ_{IS} is the anisotropy of the dipolar coupling $[\delta_{IS} = (\mu/2\pi)(\hbar\gamma_I\gamma_S/r^3)]$ and $\omega_I\Delta\sigma_I = 3/2\delta_I$ is the difference between $\omega_I\sigma_{zz}$ and $\omega_I\sigma_{xx}$, two of the principal values of the chemical-shift anisotropy (CSA) tensor (where we assume the CSA to be axially symmetric). In this study, for ^{15}N relaxation, these terms correspond to the ^{1}H–^{15}N dipole-dipole and ^{15}N CSA interactions.

A common strategy for the determination of internal dynamics in a molecule is to measure a set of relaxation-rate constants and assume a number of exponential terms describing the internal dynamics [Eq. (1)]. The correlation times (τ_k) and amplitudes (A_k) are optimized for each exponential term such that experimental relaxation-rate constants are reproduced well. For solid-state NMR, such an approach to analysis may yield a distorted representation of the internal dynamics, if the model contains fewer exponential terms than the real motion.[12]

An alternative approach is to characterize the motion with several detector responses, which quantify the motion for a range of correlation times, defined by $\rho_n(z)$ (the detector "sensitivity"), and is unbiased by any model of the correlation function. We shortly summarize this approach here (for a detailed description, see Ref. 13). Detectors are obtained via optimized linear combination of the experimental rate constants. If, for example, we take two rate constants, $R_\zeta^{(\theta,S)}$ and $R_\xi^{(\theta,S)}$, and add them together with coefficients a and b, we can define a detector response, $\rho_n^{(\theta,S)}$, as

$$\rho_n^{(\theta,S)} = aR_\zeta^{(\theta,S)} + bR_\xi^{(\theta,S)}. \tag{7}$$

We can understand why such an approach is useful, if we describe the correlation function by a distribution of correlation times of motion (henceforth referred to as the distribution of motion)

$$C(t) = \frac{1}{5}\left[S^2 + (1-S^2)\int_{-\infty}^{\infty}\theta(z)\exp(-t/(10^z\cdot 1\text{ s}))dz\right], \tag{8}$$

where $(1-S^2)$ gives the total amplitude of motion and $\theta(z)$ gives the distribution of that motion over all correlation times [$\theta(z)$ integrates

to 1], where $z = \log_{10}(\tau_c/1\text{ s})$. Then, each relaxation-rate constant is given by

$$R_\zeta^{(\theta,S)} = (1 - S^2)\int_{-\infty}^{\infty} \theta(z) R_\zeta(z) dz, \tag{9}$$

where $R_\zeta^{(\theta,S)}$ is the rate constant for an experiment, indicated by ζ, with a distribution given by $(1 - S^2)\theta(z)$. $R_\zeta(z)$ is the "sensitivity" of that experiment at a given correlation time, z, and can be calculated from Eqs. (4)–(6), by assuming a mono-exponential correlation function with correlation time $\tau_c = 10^z \cdot 1$ s and order parameter $(1 - S^2) = 1$. A glossary of the terms used here is given at the beginning of the supplementary material.

The value of $\rho_n^{(\theta,S)}$ is given by

$$\rho_n^{(\theta,S)} = (1 - S^2)\int_{-\infty}^{\infty} \theta(z) \rho_n(z) dz, \tag{10}$$

where the sensitivity of the detector, $\rho_n(z)$, is

$$\rho_n(z) = aR_\zeta(z) + bR_\xi(z). \tag{11}$$

One adjusts a and b to optimize the form of $\rho_n(z)$. This principle can be applied to large sets of experimental rate constants so that one may design the detector sensitivities, $\rho_n(z)$, to give optimally separated ranges of correlation times. In this case, we define detection vectors, $\vec{r}_n$, which relate the experimental rate constants to the detector responses as

$$\begin{pmatrix} \rho_1^{(\theta,S)} \\ \vdots \\ \rho_n^{(\theta,S)} \end{pmatrix} = \begin{pmatrix} [\vec{r}_1]_\zeta/\sigma(R_\zeta) & \cdots & [\vec{r}_n]_\zeta/\sigma(R_\zeta) \\ \vdots & \ddots & \vdots \\ [\vec{r}_1]_\xi/\sigma(R_\xi) & \cdots & [\vec{r}_n]_\xi/\sigma(R_\xi) \end{pmatrix}^{-1} \begin{pmatrix} R_\zeta^{(\theta,S)}/\sigma(R_\zeta) \\ \vdots \\ R_\xi^{(\theta,S)}/\sigma(R_\xi) \end{pmatrix}, \tag{12}$$

where $[\vec{r}_j]_\zeta$ is the element of detection vector j, corresponding to the relaxation-rate constant denoted by ζ, and the matrix power of -1 indicates a pseudoinverse (since one typically has more experiments than detectors). $\sigma(R_\zeta)$ indicates the standard deviation for the experiment denoted by ζ. Inclusion of this term reweights the linear combination depending on data quality for each experiment and residue. It may also be omitted, but its inclusion is default in the DIFRATE software.[24] Essentially, we are fitting the measured rate constants with a sum of the detection vectors. Note that, in practice, one restricts the allowed values of the detector responses so that a linear least-squares solver may be necessary for this fit, as opposed to using a simple matrix inversion as shown here.

B. Sensitivity to internal motion

The simple, linear relationship between the distribution of motions, $(1 - S^2)\theta(z)$, and the measured rate constants, $R_\zeta^{(\theta,S)}$, as obtained in Eq. (9), is particularly useful for dynamics analysis in solid-state NMR. When no tumbling is present, the correlation function primarily describes internal motion with additional contributions from small-amplitude overall motion of the protein (such as "rocking" in a crystal[26,27] or overall motion in a fibril[28]). By contrast, in solution-state NMR, the total correlation function is a product of the correlation function of the internal motion and the correlation function of the tumbling [Eq. (2), assuming statistical independence of the two motions]. Although one may apply the detector analysis as derived for solid-state NMR directly to solution-state data, the resulting detector responses convolute information about the distribution of internal motion with information about the overall tumbling (see below). We would rather characterize only the distribution of internal motion which requires a similar relationship between the measured rate constants, $R_\zeta^{(\theta,S)}$, and the distribution of internal motion [denoted as $(1 - S^2)\theta(z_i)$, where z_i is the log of the internal correlation time, $z_i = \log_{10}(\tau_i/1\text{ s})$].

To do so, we begin with the correlation function of an interaction in a molecule undergoing isotropic molecular tumbling and internal motion described by a distribution $(1 - S^2)\theta(z_i)$, which is given by

$$C(t) = \frac{1}{5}\exp(-t/\tau_r)\left[S^2 + (1 - S^2)\int_{-\infty}^{\infty} \theta(z_i)\exp(-t/(10^{z_i} \cdot 1\text{ s}))dz_i\right]. \tag{13}$$

In analogy to Eq. (9), this leads to a solution-state relaxation-rate constant of the form

$$R_\zeta^{(\theta,S)} = S^2 R_\zeta(z_r) + (1 - S^2)\int_{-\infty}^{\infty} \theta(z_i) R_\zeta(z_{\text{eff}}(z_i))dz_i. \tag{14}$$

Here, $z_r = \log_{10}(\tau_r/1\text{ s})$, and the effective correlation time describing the combined effects of overall and internal motion is given by

$$\tau_{\text{eff}} = \frac{\tau_i \tau_r}{\tau_i + \tau_r}. \tag{15}$$

The dependence of τ_{eff} as a function of τ_i is plotted in Fig. 3. If we take $z_{\text{eff}} = \log_{10}(\tau_{\text{eff}}/1\text{ s})$, we obtain

$$z_{\text{eff}}(z) = \log_{10}\left(\frac{\tau_r 10^{z_i}}{\tau_r + 10^{z_i} \cdot 1\text{ s}}\right). \tag{16}$$

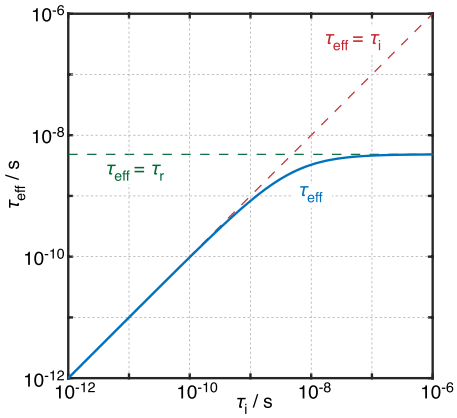

FIG. 3. Effective correlation time for internal motions. The effective correlation time, τ_{eff}, is plotted against the internal correlation time, τ_i, assuming a rotational correlation time of $\tau_r = 4.84$ ns. We show the effective correlation time τ_{eff} (solid blue line), the correlation time for internal motions, τ_i (red dashed line), and the rotational correlation time, τ_r (green dashed line). If $\tau_i \ll \tau_r$, then $\tau_{\text{eff}} = \tau_i$, but as τ_i approaches τ_r the effective correlation time evolves asymptotically toward τ_r.

We can now rewrite the solution-state relaxation-rate constant such that the effect of overall rotational tumbling is separated from the net effects of the distribution of internal motion, $(1-S^2)\theta(z_i)$,

$$R_\zeta^{(\theta,S)} = S^2 R_\zeta(z_r) + (1-S^2)\int_{-\infty}^{\infty}\theta(z_i)R_\zeta(z_{eff}(z_i))dz_i$$
$$= R_\zeta^0 + (1-S^2)\int_{-\infty}^{\infty}\theta(z_i)\left(R_\zeta(z_{eff}(z_i)) - R_\zeta^0\right)dz_i, \quad (17)$$

where we have defined $R_\zeta^0 = R_\zeta(z_r)$. Then, if we define the sensitivity to internal motion as

$$R_\zeta^{solu.}(z_i) = R_\zeta(z_{eff}(z_i)) - R_\zeta^0 = R_\zeta\left(\log_{10}\left(\frac{\tau_r 10^{z_i}}{\tau_r + 10^{z_i}\cdot 1\ s}\right)\right) - R_\zeta^0, \quad (18)$$

we obtain the following formula for the relaxation-rate constant:

$$R_\zeta^{(\theta,S)} = R_\zeta^0 + (1-S^2)\int_{-\infty}^{\infty}\theta(z_i)R_\zeta^{solu.}(z_i)dz_i. \quad (19)$$

The resulting equation has nearly the same form as Eq. (9), with the only differences between Eqs. (18) and (9) being the offset term, R_ζ^0, and that we first calculate the effective correlation time from z_i and τ_r, which is then inserted into the sensitivity, as $R_\zeta(z_{eff}(z_i))$. Note that in this study, we assume isotropic tumbling throughout. In principle, one may also introduce a more complex form of the correlation function of the tumbling in Eq. (13), as would result from anisotropic tumbling. This will result in different experimental sensitivities to internal motion, $R_\zeta^{solu.}(z_i)$, depending on the relative orientation of the rotational diffusion tensor and the corresponding bond. While this will make the optimization of detector sensitivities more complicated, variations in the experimental sensitivities will not prohibit the application of detectors unless the anisotropy is extreme. It is possible to generate very similar detector sensitivities for all orientations for the range $0.2 \le D_\parallel/D_\perp \le 5$, where variation in experimental sensitivity will require reoptimization of detector sensitivities for each bond orientation, although this step can be automated. For larger anisotropies, detector sensitivities for different residues may be significantly different so that the detector responses themselves should not be directly compared (detector analysis may still be applied, but attention must be given to changes in sensitivities).

We can decompose the contributions to the relaxation-rate constant given in Eqs. (18) and (19) into three parts, as illustrated in Fig. 4, which depend on the internal distribution of motion, $(1-S^2)\theta(z_i)$, and the correlation time of the tumbling, τ_r: (i) Relaxation induced by tumbling alone, as in the case of a completely rigid molecule. (ii) Reduction of relaxation from tumbling due to attenuation of NMR interactions by internal motion. (iii) Relaxation induced directly by the effective internal motion [see Eq. (18)].

The separation into three contributions seems at first slightly counterintuitive: we expect tumbling to mask the influence of motions with correlation times significantly longer than τ_r. The attenuation of NMR interactions by internal motions ($\delta_{eff} = S\delta$) can be considered uniform for all correlation times (subtracting R_ζ^0 from the sensitivity), while relaxation induced directly by internal motion [adding $R_\zeta(z_{eff}(z_i))$ to the sensitivity] depends on z_i but approaches R_ζ^0 for long correlation times. However, the sum of the latter two contributions is 0 for long correlation times, yielding the expected behavior. This is equivalent to the usual description: internal motions much slower than the overall tumbling are not relaxation active.

In principle, it is also possible to characterize the solution-state relaxation-rate constants using the methodology developed for solid-state NMR. However, such an analysis would provide the total distribution of motion, $\theta_{tot.}(z)$, which yields the correlation function via Eq. (8). This distribution describes the internal motion (having an effective correlation time as opposed to the internal correlation time) and the overall tumbling motion. Since the overall tumbling leads to an isotropic distribution of orientations, the order parameter is then $S^2 = 0$ such that $(1-S^2) = 1$, and we obtain

$$R_\zeta^{(\theta,S)} = R_\zeta^0 + (1-S^2)\int_{-\infty}^{\infty}\theta(z_i)R_\zeta^{solu.}(z_i)dz_i$$
$$= R_\zeta^{(\theta_{tot.},0)} = \int_{-\infty}^{\infty}\theta_{tot.}(z)R_\zeta(z)dz. \quad (20)$$

The distribution of total motion, $\theta_{tot.}(z)$, is different from the distribution of internal motion, $(1-S^2)\theta(z_i)$, since overall tumbling ($z = z_r$) and internal motion ($z = z_{eff}$) contribute to the distribution of total motion [for $\theta_{tot.}(z)$, z can be both the tumbling correlation time, z_r, and z_{eff}, resulting from internal motion and tumbling]. Note that there is a well-defined relationship between the two distributions, given in supplementary material, Sec. 1.

We investigate the behavior of the sensitivity to internal motion [$R_\zeta^{solu.}(z_i)$] by considering several typical sets of experiments. For example, Fig. 5(a) shows the normalized sensitivities, $R_\zeta(z)$, to the distribution of the total motion, $\theta_{tot.}(z)$, for R_1, R_2, and σ_{NH} rate constants. In Fig. 5(b), normalized sensitivities, $R_\zeta^{solu.}(z_i)$, to the distribution of the internal motion, $(1-S^2)\theta(z_i)$, are given. We see a number of differences: first, at short correlation times, the sensitivities to internal motion, $R_\zeta^{solu.}(z_i)$, are negative due to the correction term R_ζ^0 [see Eq. (18)]. At sufficiently short correlation times, very little relaxation is induced directly by internal motion, and the sensitivity is dominated by the term $-R_\zeta^0$ in Eq. (18), resulting in a reduction of the relaxation-rate constant compared to a rigid molecule. At longer correlation times, the sensitivity to internal motion increases and, in some cases, becomes positive, but when the internal correlation time becomes larger than the correlation time of the overall tumbling, all the $R_\zeta^{solu.}(z_i)$ approach zero since the tumbling masks internal motions that are significantly slower than the tumbling. The sensitivity of the R_1 rate constant varies significantly in the range 600–950 MHz [Fig. 5(c)], with less variation for the sensitivity σ_{NH}, and almost no variation for R_2 in the same range of magnetic fields.

C. Optimized linear combinations for detector design

Dynamics detectors are generated by optimizing a linear combination of the relaxation-rate constant sensitivities to obtain

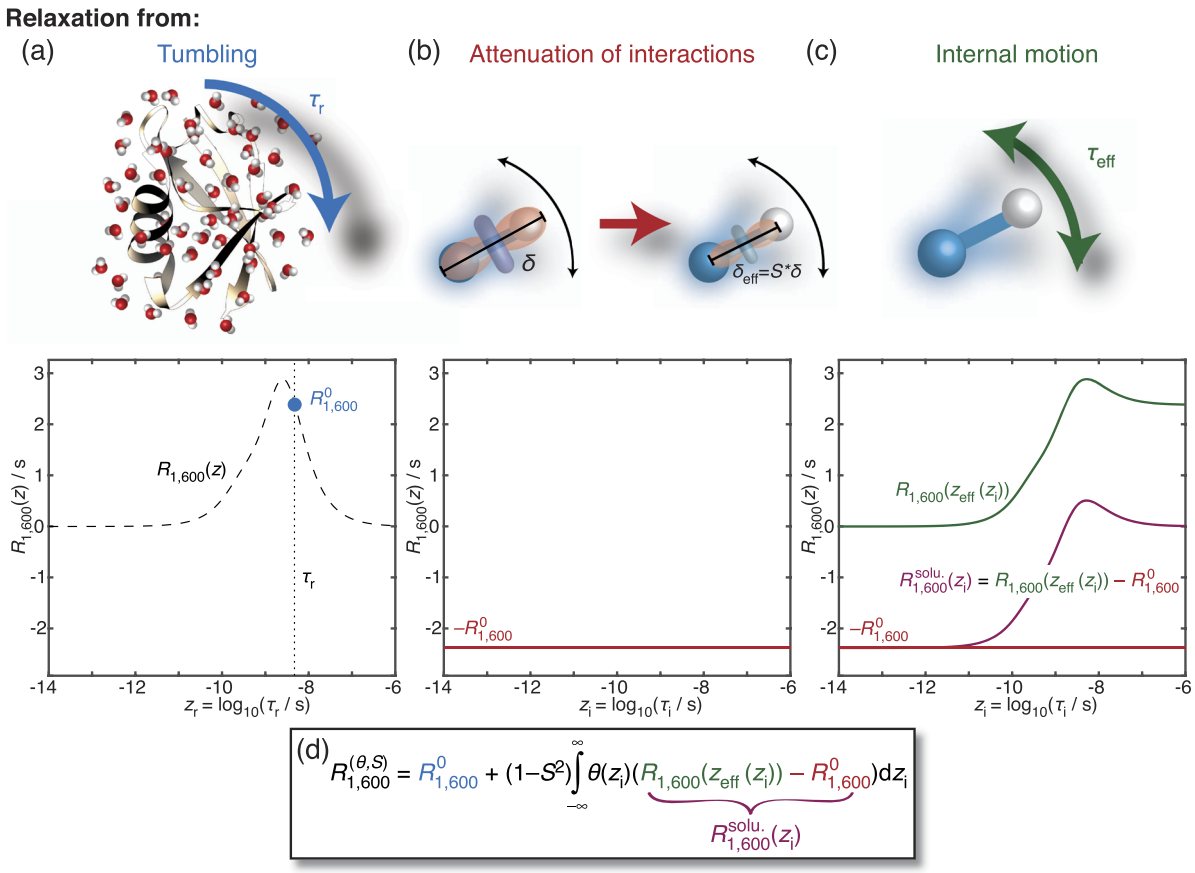

FIG. 4. Contributions to the ^{15}N R_1 relaxation-rate constant at 600 MHz with τ_r = 4.84 ns. (a) Relaxation due to tumbling for an internally rigid molecule may be calculated by evaluating $R_{1,600}(z_r) = R^0_{1,600}$, where $z_r = \log_{10}(\tau_r/1\text{ s})$. Then, (a) shows $R_{1,600}(z)$ as a dashed line, and $z_r = \log_{10}(\tau_r)$ as a vertical, dotted line, with the resulting $R^0_{1,600}$ shown as a blue circle. $R^0_{1,600}$ appears as a constant offset for calculation of the relaxation-rate constant, $R^{(\theta,S)}_{1,600}$ [see (d)]. (b) Internal motion results in a reduction of the effective size of anisotropic interactions such that $\delta_{eff} = S\delta$ [(b), top], yielding a reduction in relaxation by $(1 - S^2)R^0_{1,600}$. This reduction is scaled by the total internal motion, $(1 - S^2)$, but does not depend on the correlation time, resulting in a uniform, negative contribution to the sensitivity to internal motion of $-R^0_{1,600}$. (c) The effective internal motion (internal motion composed with tumbling) induces some relaxation directly, although with an effective correlation time [$z_{eff} = \log_{10}(\tau_{eff}/1\text{ s})$], illustrated in (c) with $R_{1,600}(z_{eff}(z_i))$ plotted [z_{eff} is a function of z and z_r, see Eq. (16) and Fig. 3]. The sensitivity to internal motion, $R^{solu.}_{1,600}(z_i)$, is finally obtained by summing $R_{1,600}(z_{eff}(z_i))$ and $-R^0_{1,600}$, which is plotted in magenta. This function along with the distribution of motion [$(1 - S^2)\theta(z_i)$] may then be used to calculate the relaxation rate constant, $R^{(\theta,S)}_{1,600}$, as given in (d). Note that for correlation times much longer than the tumbling correlation time, the terms $-R^0_{1,600}$ and $R_{1,600}(z_{eff}(z_i))$ cancel out, illustrating the fact that the tumbling masks the influence of motions with correlation times much longer than the correlation time of the tumbling.

detector sensitivities, which are well separated into different ranges of correlation times. Optimized linear combinations for the relaxation-rate constant sensitivities shown in Fig. 5 (top) were generated and plotted in Fig. 5 (bottom). Note that optimization methods discussed for solid-state NMR[13] are applicable to those used in solution-state NMR, despite the appearance of negative sensitivities.

The detector sensitivities of total and internal motion differ markedly for short and long correlation times [Figs. 5(a)/5(c) vs Figs. 5(b)/5(d), bottom]. Considering the analysis of relaxation-rate constants measured at a single magnetic field [Fig. 5(a) and (b)], we find two of the three detectors in approximately the same positions for total and internal motion (corresponding detectors are plotted with the same color). However, the third detector (ρ_3 for total motion, ρ_1 for internal motion) has moved significantly. $\rho_3(z)$ for the total motion is strongly dependent on R_2 and diverges as one approaches long correlation times, whereas $\rho^{solu.}_1(z_i)$ of the internal motion is nearly uniformly sensitive at short correlation times. Differences arise because the detectors characterize different distributions of motion [internal motion, $(1 - S^2)\theta(z_i)$, or total motion $\theta_{tot.}(z)$, see supplementary material, Sec. 1 for comparison]. The sensitivity to internal motion is altered by the tumbling, which masks slow motions. As a consequence, the sensitivities, $\rho^{solu.}_n(z_i)$, must approach zero above the overall tumbling

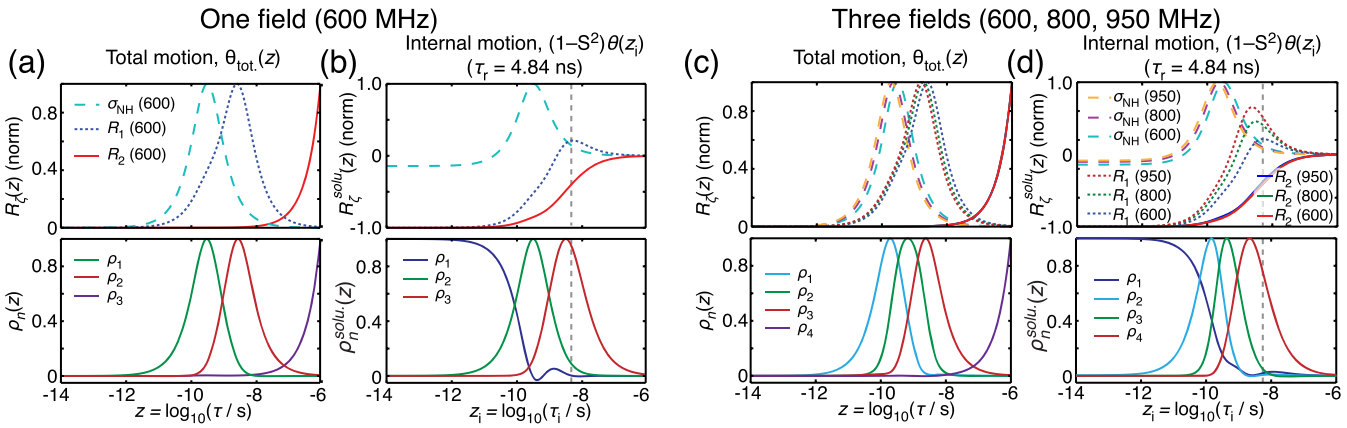

FIG. 5. Experimental sensitivities for total $[R_\zeta(z)]$ and internal $[R_\zeta^{solu.}(z_i)]$ motions, and optimized detector sensitivities $[\rho_n(z)]$. (a) Experimental sensitivities, $R_\zeta(z)$, for σ_{NH}, R_1, and R_2 rate constants at 600 MHz for the total motion (top, with sensitivities normalized to 1) and an optimized set of detector sensitivities, $\rho_n(z)$, obtained by linear combination of the rate constant sensitivities (bottom). (b) Sensitivity to internal motion, $R_\zeta^{solu.}(z_i)$, calculated assuming a tumbling correlation time of τ_r = 4.84 ns (top) and resulting detector sensitivities, $\rho_n^{solu.}(z_i)$ (bottom). (c) shows experimental sensitivities, $R_\zeta(z)$, at 600, 800 MHz, and 950 MHz for the total motion (top), with a set of four detector sensitivities, $\rho_n(z)$, calculated (bottom). (d) The same set of experiments with sensitivities to internal motion $R_\zeta^{solu.}(z_i)$ (τ_r = 4.84 ns). In (b) and (d), τ_r is indicated with a gray dotted line through all plots. In each section, the experimental sensitivities are normalized so that the maximum of the absolute value is 1. Note that the normalization of the R_2 sensitivity to the total motion, $R_2(z)$, is determined by the longest correlation time in the plot so that decreasing the maximum z in plots in (a) and (c) would cause $R_2(z)$ to appear to shift to the left [correspondingly, $\rho_3(z)$ would also shift].

correlation time. On the other hand, $\rho_n^{solu.}(z_i)$ is sensitive to motion at short correlation times since one can determine how much the measured relaxation-rate constants have been reduced from the expected relaxation for an internally rigid molecule (due to attenuation of the effective size of anisotropic interactions). Note that this can be determined because we consider the correlation time of the tumbling determined independently. The overall tumbling correlation time must be determined before detector analysis, using existing methods, e.g., the program ROTDIF[29] was used in this study.

Similar behavior is observed in the analysis of relaxation at three magnetic fields [Figs. 5(c)/5(d), bottom]. In principle, up to nine detectors can be optimized for nine relaxation rate constants. However, R_2 sensitivities are typically very similar so that one rarely gains additional discrimination between correlation-time ranges by using more than one R_2 experiment. Multiple R_2 experiments are nonetheless useful because they increase the signal-to-noise ratio and allow the determination of contributions of broadening due to fast chemical exchange to R_2 (see below). Similarly, multiple high-field R_1 usually only provide two detectors, as do multiple NOE experiments (although sufficient separation in B_0 fields and signal-to-noise may allow more). Such a three-field data set can be used to optimize three to five detectors, depending on the signal-to-noise ratio and the separation of the B_0 fields. Here, we have optimized four detectors (supplementary material, Sec. 2.3 discusses the choice of number of detectors). The range of sensitivities barely increases from one to three fields (considering detectors ρ_2–ρ_4; ρ_1 is always sensitive to the shortest correlation times for solution-state data). This is because the shortest correlation times to which ρ_2 is sensitive are determined by the highest field at which the NOE (σ_{NH}) was measured, and the sensitivity to long correlation times is limited by the rotational correlation time (as opposed to the choice of the experimental parameters). So, it is possible to shift $\rho_2^{solu.}(z_i)$ toward shorter correlation times, by using a larger B_0 field for the NOE experiment, but sensitivity to longer correlation times can only be significantly increased if the rotational correlation time becomes longer and the magnetic field, B_0, becomes lower. Changing the B_0 field within the range of high fields used in biomolecular NMR has very limited effect since the variations of sensitivity of different σ_{NH} are relatively small compared to the difference in sensitivity of σ_{NH} and R_1 at the same field.

We have previously developed a graphical method of optimization to generate detector sensitivities from linear combinations of the relaxation-rate constant sensitivities, using "allowed spaces."[13] Here, we simply review the definition of the spaces and how they are used to generate the linear combination of relaxation-rate constant sensitivities. An allowed space can be understood as follows: suppose we record a set of N experiments. Then, we can take an N-dimensional space, where each axis represents the value of one of the relaxation-rate constants. Not all combinations of relaxation-rate constants are physically possible given an arbitrary distribution of motion, $(1 - S^2)\theta(z)$, so that we may determine what points in the space correspond to a set of relaxation-rate constants that can result from some distribution of motion. All possible sets of rate constants for an arbitrary distribution of motion are then referred to as the "allowed space." Note that for solution-state relaxation, a molecule with no internal motion will still have nonzero relaxation-rate constants due to overall tumbling [Eq. (17)]. Therefore, when plotting the allowed space for solution-state relaxation, we first calculate $R_\zeta^{(\theta,S)} - R_\zeta^0$ so that the origin of the space corresponds to no internal motion ($1 - S^2 = 0$). We also use rate constants with normalized axes denoted as $\Re_\zeta^{(\theta,S)}$, where ζ indicates the experiment, to yield

$$\begin{aligned}\mathfrak{R}_\zeta^{(\theta,S)} &= (R_\zeta^{(\theta,S)} - R_\zeta^0)/c_\zeta,\\ c_\zeta &= \text{median}(\sigma(R_\zeta)),\\ &\quad or\\ c_\zeta &= \max\left|R_\zeta^{\text{solu.}}(z)\right|.\end{aligned} \tag{21}$$

In the case that one plots the allowed space for a particular set of experimental measurements, c_ζ can be taken to be the standard deviation of the measurement of rate constant, $R_\zeta^{(\theta,S)}$, or its median for a rate constant measured at multiple sites. The distance between two points in the allowed space quantifies how easily these points may be distinguished from the given experimental data set. In the absence of experimental data, one can take the maximum of the absolute value of the sensitivity to internal motion so that all experiments are on a similar scale.

The allowed space of relaxation-rate constants for a data set including R_1, R_2, and σ_{NH} at a single field (at 600 MHz, taking $c_\zeta = \max\left|R_\zeta(z)\right|$) was computed (see Fig. 6). The origin corresponds to no internal motion ($1 - S^2 = 0$). The observed relaxation-rate constants at the origin are nonzero due to the offset terms, R_ζ^0, as indicated in Eq. (21). Positions in the space that can result from internal motion with a single correlation time (Dirac distribution) are shown as solid lines (see Fig. 6 with $1 - S^2 = 1$ and $1 - S^2 = 0.5$). The volume shown corresponds to any point that can be constructed from a (positive) linear combination of positions in the space corresponding to single correlation times, i.e., any point that can result from some distribution of internal motion, $(1 - S^2)\theta(z_i)$.

We note that for a given data set, the information about how motion is distributed over different internal correlation times, as described by $\theta(z_i)$, is contained entirely in the ratios of the various rate constants, whereas the total amplitude of motion, $(1 - S^2)$, is obtained from the magnitude of the rate constants. Therefore, we have introduced a "reduced space" of rate constants, for which we define a ratio of the relaxation-rate constants, in order to remove dependence on the total amplitude of motion (reducing the dimensionality has practical advantages, in particular, allowing one to visualize the allowed space of rate constants for three rate constants in a 2D plot). Previously, we have defined the dimensions of the reduced space to be given by some $\kappa_\zeta = \mathfrak{R}_\zeta^{(\theta,S)}/\Sigma_\zeta\mathfrak{R}_\zeta^{(\theta,S)}$, where $\Sigma_\zeta\mathfrak{R}_\zeta^{(\theta,S)}$ indicates the sum of all normalized relaxation rate constants. For N experiments, one obtains then $N - 1$ linearly independent κ_ζ to define the reduced space. When defining the κ_ζ for solution-state analysis, however, we must be careful because the $\mathfrak{R}_\zeta^{(\theta,S)}$ can be both negative and positive so that $\Sigma_\zeta\mathfrak{R}_\zeta^{(\theta,S)}$ may cross zero, causing κ_ζ to diverge at such points. Therefore, we use one of the experiments, ζ, for which the corresponding sensitivity, $R_\zeta^{\text{solu.}}(z_i)$, remains negative at all values of z_i to define the reduced space. Such a behavior is often observed for relaxation-rate constants which sample the spectral density at zero frequency [$J(0)$], i.e., transverse relaxation-rate constants. For the example shown above with relaxation-rate constants R_1, R_2, and σ_{NH} at 600 MHz, the corresponding reduced space can be defined by dividing by $\mathfrak{R}_{2,600}^{(\theta,S)}$ so that

$$\kappa_{R1,600} = \frac{\mathfrak{R}_{R1,600}^{(\theta,S)}}{-\mathfrak{R}_{R2,600}^{(\theta,S)}}, \quad \kappa_{\sigma,600} = \frac{\mathfrak{R}_{\sigma,600}^{(\theta,S)}}{-\mathfrak{R}_{R2,600}^{(\theta,S)}}, \tag{22}$$

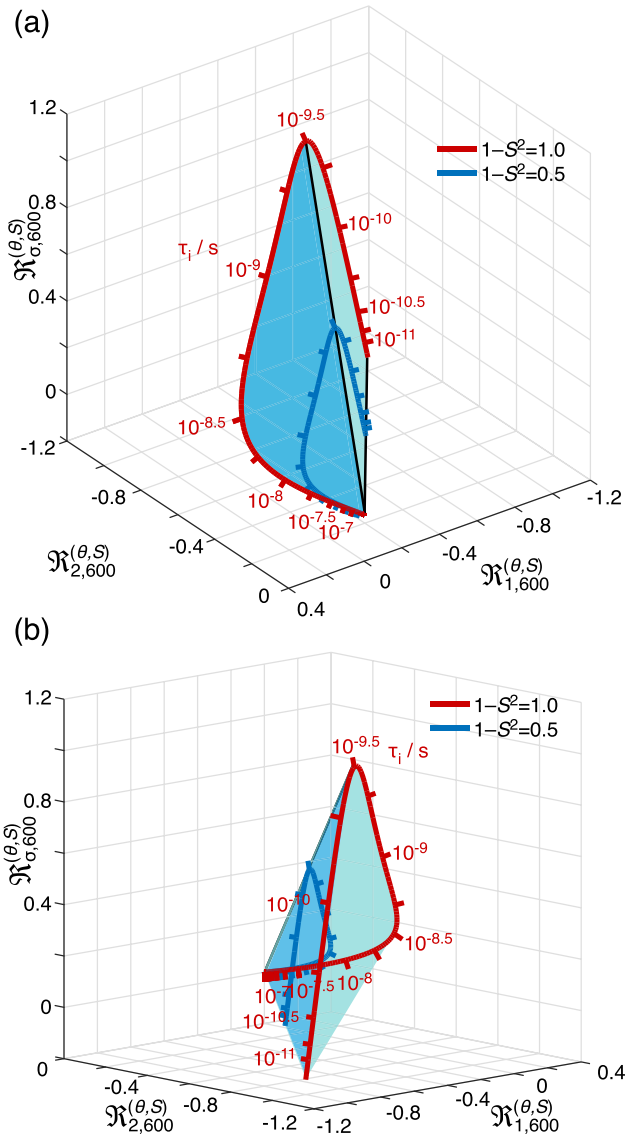

FIG. 6. Allowed space of normalized rate constants for ^{15}N R_1, R_2, and σ_{HN} rate constants acquired at 600 MHz, assuming τ_r = 4.84 ns. Two views are shown in (a) and (b), where the axes are the normalized rate constants, $\mathfrak{R}_\zeta^{(\theta,S)}$. Sets of the three rate constants which are possible for an arbitrary distribution of internal motion, $(1 - S^2)\theta(z_i)$, are highlighted in blue (allowed space, different shading shows different sides of the space). Traces show positions in the space corresponding to exactly one correlation time, with the red trace having an order parameter, S^2, such that $(1 - S^2)$ = 1 and blue having an order parameter such that $(1 - S^2)$ = 0.5. Note that the allowed space is a volume and contains all points that are along the red trace and additionally all points that are between two or more points on the red trace.

where the dimensionality of the reduced space is one less than the number of experiments. An example of the reduced space is shown for R_1, R_2, and σ_{NH} at 600 MHz, for both the total motion (includes tumbling in solution) and the internal motion (tumbling removed) in Figs. 7(a) and 7(b), respectively.

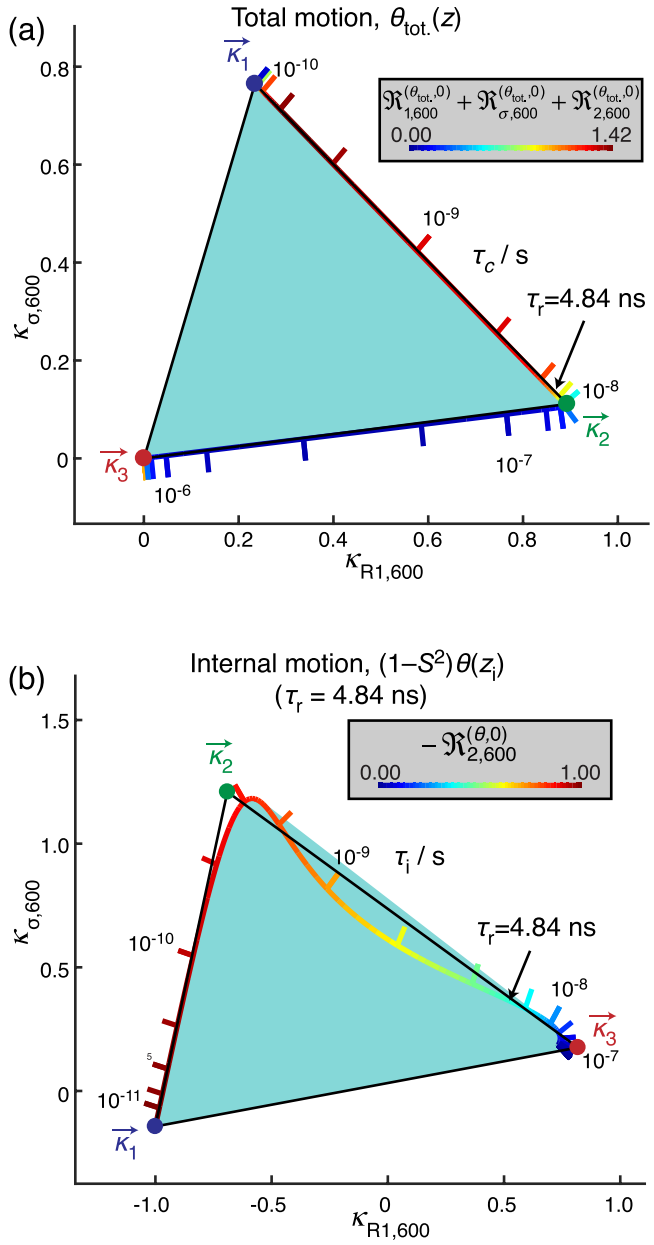

FIG. 7. Reduced space of normalized rate constants for R_1, R_2, and σ_{NH} rate constants at 600 MHz, where the x- and y-axes correspond to κ. (a) Allowed region (cyan) for the sensitivities to the total motion [for characterizing $\theta_{tot.}(z)$, see Eq. (20)], where κ are obtained by dividing by $\Re^{(\theta_{tot.},S)}_{1,600} + \Re^{(\theta_{tot.},S)}_{\sigma,600} + \Re^{(\theta_{tot.},S)}_{2,600}$ (this value is color-coded onto the plot for $S = 0$ when the position corresponds to a single correlation time). (b) Allowed region (cyan) for the sensitivities to the internal motion [$(1 - S^2)\theta(z_i)$, assuming τ_r = 4.84 ns], where the κ coefficients are obtained by dividing by $-\Re^{(\theta,S)}_{2,600}$ (value color-coded onto the plot for $S = 0$ when the position corresponds to a single internal correlation time). In both (a) and (b), good positions for $\vec{\kappa}_n$ are shown as colored dots, which indicate the direction of the detection vectors ($\vec{r}_n$). These correspond to the sensitivities shown in Figs. 5(a) and 5(b), respectively, after applying normalization [for example, see Eq. (23)].

Detectors are generated by selecting an optimal set of "detection vectors" that extend into the full space. Correspondingly, these are points in the reduced space (their positions denoted as $\vec{\kappa}_n$). From these positions, it is possible to determine the direction of the detection vector, in this example defined by $\kappa_{R1,600}$ and $\kappa_{\sigma,600}$, according to

$$\vec{r}_n = \boldsymbol{a_n} \begin{pmatrix} \boldsymbol{\kappa}_{R2,600}\boldsymbol{c}_{R2,600} \\ \boldsymbol{\kappa}_{R1,600}\boldsymbol{c}_{R1,600} \\ \boldsymbol{\kappa}_{\sigma,600}\boldsymbol{c}_{\sigma,600} \end{pmatrix}, \quad \boldsymbol{\kappa}_{R2,600} = -1. \tag{23}$$

Recall that the κ_ζ define ratios of the rate constants, but not their absolute values, so that a point in the reduced space ($\vec{\kappa}_n$) does not define the length of the detection vector, only its direction. The length is then determined by adjustment of a_n, which changes the amplitude of the corresponding detector sensitivity since it is inversely proportional to a_n (as discussed previously;[13] we use the equal-maximum normalization here, with all sensitivities having maxima of one). Ideally, one surrounds (or nearly surrounds) the reduced space with a minimal number of $\vec{\kappa}_n$. To fully surround the space, it is necessary to have at least N different $\vec{\kappa}_n$ for N experiments. However, one may also reduce the number of $\vec{\kappa}_n$, yielding fewer detectors, but obtain a more precise determination of the remaining detectors.[13] The colored dots in Figs. 7(a) and 7(b) indicate good choices for $\vec{\kappa}_n$ to yield well-separated detector sensitivities, for the total motion (solid-state) and internal motion (solution-state), respectively. The positions yield the detector sensitivities shown in Figs. 5(a) and 5(b) (bottom).

As in Eq. (12), measured relaxation-rate constants in solution-state are fitted to detection vectors, $\vec{r}_n$. For solution-state data, due to the offset term, R^0_ζ, appearing in Eq. (21), the calculated detector responses are given by

$$\begin{pmatrix} \rho_1^{(\theta,S)} \\ \vdots \\ \rho_n^{(\theta,S)} \end{pmatrix} = \begin{pmatrix} [\vec{r}_1]_\zeta/\sigma(R_\zeta) & \cdots & [\vec{r}_n]_\zeta/\sigma(R_\zeta) \\ \vdots & \ddots & \vdots \\ [\vec{r}_1]_\xi/\sigma(R_\xi) & \cdots & [\vec{r}_n]_\xi/\sigma(R_\xi) \end{pmatrix}^{-1} \times \begin{pmatrix} (R_\zeta^{(\theta,S)} - R_\zeta^0)/\sigma(R_\zeta) \\ \vdots \\ (R_\xi^{(\theta,S)} - R_\xi^0)/\sigma(R_\xi) \end{pmatrix}. \tag{24}$$

Here, the variables ζ to ξ span the experimental data set (e.g., for a one field data set at 600 MHz, the ζ, ξ would be replaced by $R_{2,600}$, $R_{1,600}$, σ_{600}). Before fitting, one subtracts R^0_ζ from each experimental rate constant. Note that the number of detection vectors cannot exceed the number of experiments, and in practice, there are usually fewer detection vectors than experiments. In particular, when experiments have similar sensitivities, the use of too many detection vectors would result in some of them being almost colinear so that the matrix shown in Eq. (24) would be almost singular (i.e., lacking an inverse) increasing the error of the analysis (see supplementary material, Sec. 2.2 for more details). One also obtains the detector sensitivities from the detection vectors, which results in a similar

expression as in Eq. (24),

$$\begin{pmatrix} \rho_1^{solu.}(z) \\ \vdots \\ \rho_n^{solu.}(z) \end{pmatrix} = \begin{pmatrix} [\vec{r}_1]_\zeta/\sigma(R_\zeta) & \cdots & [\vec{r}_n]_\zeta/\sigma(R_\zeta) \\ \vdots & \ddots & \vdots \\ [\vec{r}_1]_\xi/\sigma(R_\xi) & \cdots & [\vec{r}_n]_\xi/\sigma(R_\xi) \end{pmatrix}^{-1} \times \begin{pmatrix} R_\zeta^{solu.}(z)/\sigma(R_\zeta) \\ \vdots \\ R_\xi^{solu.}(z)/\sigma(R_\xi) \end{pmatrix}. \quad (25)$$

Note that we have modified Eq. (25) slightly from its previous form, where normalization by the standard deviations, $\sigma(R_\zeta)$, was not indicated.[13] This usually makes little difference in the resulting sensitivities but is a more rigorous definition in the case that standard deviations are included when fitting the rate constants as in Eq. (24).

Although allowed spaces may be used for visualization of the information content of a relaxation data set, and subsequent placement of detection vectors, $\vec{r}_n$ (via the placement of $\vec{\kappa}_n$ in the reduced space), to generate optimized linear combinations of rate constants, this method may become cumbersome for large data sets. A solution is to use singular value decomposition[30] for detector optimization (see supplementary material, Sec. 2.1). One can also estimate detector uncertainties as a function of the resulting singular values (supplementary material, Secs. 2.2 and 2.3). Tools to perform this optimization and subsequent analysis are provided in DIFRATE version 2,[24] which is available for MATLAB (also available without a MATLAB license via MATLAB Runtime). In the analysis of typical ^{15}N relaxation data sets presented below, we have used this improved approach.

D. Correcting for exchange contributions

Thus far, we have assumed that all contributions to the measured relaxation-rate constants can be explained by the distribution of motion [Eq. (20)], describing internal stochastic motion, and by overall tumbling of the molecule in solution. However, other sources of relaxation may exist, in particular, the contribution of exchange to transverse relaxation rates, R_2. In this case, we must also account for such a process in our analysis. The analysis of picosecond-nanosecond motion can be performed with data at multiple magnetic fields. If the exchange process is in the fast-exchange regime $[2\pi(\nu_1 - \nu_2)\tau_{ex} \ll 1]$, where ν_1 and ν_2 are the two resonance frequencies of the exchanging resonance, R_2 is proportional to $(\nu_1 - \nu_2)^2$, which is in turn proportional to B_0^2. In this case, one can add an additional detection vector with nonzero terms corresponding to each R_2 experiment, which are proportional to B_0^2. For example,

$$\vec{r}_{ex} = \begin{pmatrix} 0 \\ \vdots \\ \boldsymbol{B}_{0,\xi}^2 \\ \vdots \\ \boldsymbol{B}_{0,\zeta}^2 \\ 0 \\ \vdots \end{pmatrix} / \boldsymbol{B}_{0,\xi}^2 \quad (26)$$

could be added to a set of detection vectors where $B_{0,\zeta}^2$ give the static magnetic fields of the R_2 experiments. Then, this detection vector is also fitted to the data with the rest of the detection vectors and will fit deviations of R_2 relaxation behavior due to fast exchange contributions. Normalization of this detection vector will not affect our ability to factor out the influence from chemical exchange. However, in the normalization scheme here, we set one of the elements to one so that the responses of this detector will estimate $R_{2,ex}$ at the field corresponding to this element. This method of accounting for chemical exchange is only applicable with R_2 acquired at multiple fields. Note that there is no corresponding sensitivity function $[\rho_n(z)]$ for this detector.

III. RESULTS AND DISCUSSION

We have applied detectors derived from simple one-field or typical multifield data sets (three fields) to relaxation data previously acquired on ubiquitin in solution-state NMR[31] (Fig. 8). The rotational correlation time was determined previously, using the ROTDIF software.[29] The analysis of relaxation data acquired at two fields is shown in supplementary material, Sec. 3. The results obtained with relaxation rates measured at one or three magnetic fields are similar. ρ_1 (<~100 ps) yields relatively uniform behavior for both one- and three-field data sets, with more motion at the C-terminus. ρ_3 (one field, ~4 ns) and ρ_4 (three fields, ~3 ns) also exhibit similar behavior for both analyses (we indicate the approximate center of the detector in parentheses, where the widths cover just over an order of magnitude). Uncertainties are slightly smaller for ρ_1 and significantly smaller for ρ_4 in the three-field analysis (ρ_4 compared to ρ_3 in the one-field analysis), which simply results from the use of more data (and therefore better signal-to-noise) in the three-field analysis and not the inclusion of new information. ρ_2 (one-field, ~250 ps) and ρ_2/ρ_3 (three-field, ~100/500 ps) show increased motion around residues 7–13 (β1-β2 turn), as well as more motion at the C-terminus, with relatively little motion elsewhere. Motion measured with ρ_2 when using only one field is split between the two detectors ρ_2 and ρ_3 when combining data from three fields, although splitting this detector results in larger uncertainties (the choice of number of detectors using three fields is investigated with variants of the Akaike information criterion[32–36] in supplementary material, Sec. 4). In the multifield data set, we have also accounted for exchange contributions to R_2 relaxation,[1] by including an additional detector that fits fast exchange (such that $R_{2,ex} \propto {B_0}^2$). This removes several distortions due to exchange, appearing primarily in $\rho_1^{(\theta,S)}$ (residues 23, 25, 70), where residues exhibiting significant exchange contributions to R_2 are consistent with previous studies.[37,38] Overall, we obtain an accurate dynamics detector analysis with separation of ranges of correlation times from typical high-field data sets.

In the current analysis, we have neglected the anisotropy of the rotational diffusion tensor. Previously, the anisotropy under these experimental conditions was determined to be small with $D_\parallel/D_\perp = 1.18$[31] so that the overall correlation function $[C_O(t)]$ decays slightly slower for H–N bonds in ubiquitin parallel to the z-component of the diffusion tensor in its principle axis system (PAS) and slightly faster for H–N bonds perpendicular to the z-component. This means that the correction terms, R_ζ^0, may not

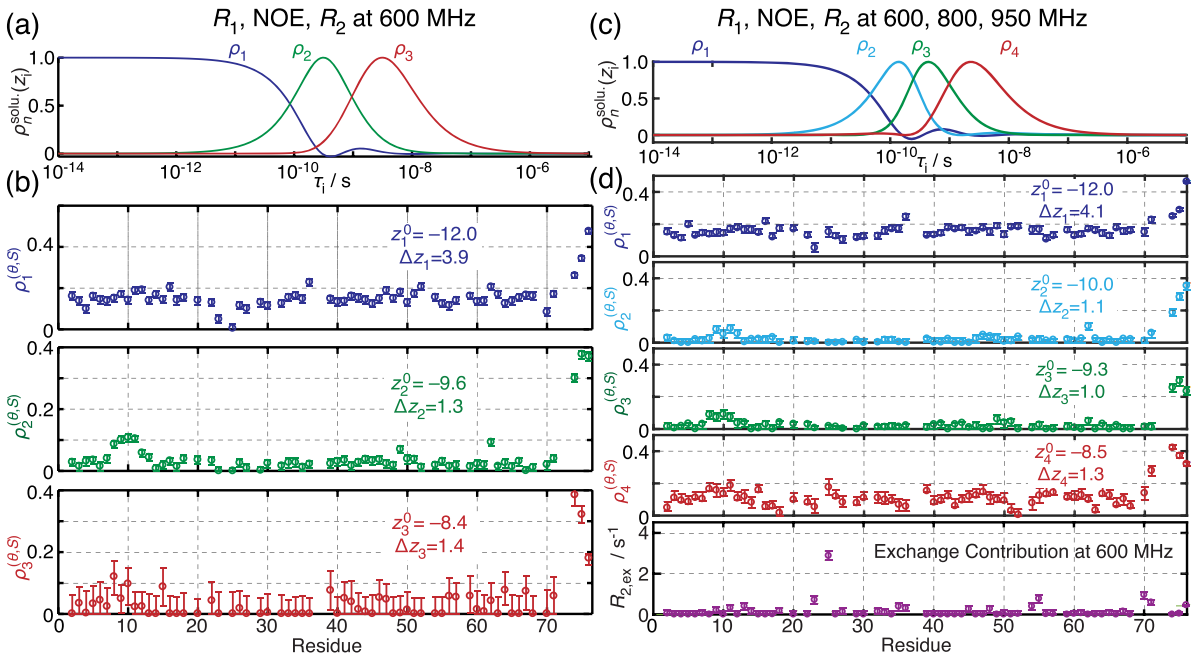

FIG. 8. Detector responses for ubiquitin from R_1, σ_{NH}, and R_2 relaxation-rate constants acquired at one or three magnetic fields. (a) shows the detector sensitivities $[\rho_n^{solu.}(z_i)]$ calculated from R_1, σ_{NH}, and R_2 rate constants at one field (600 MHz, definition of detection vectors in supplementary material, Table S2). (b) shows the experimental detector responses from data at this single field. (c) shows sensitivities calculated from relaxation-rate constants measured at three fields (600, 800, 950 MHz, definition of detection vectors in supplementary material, Table S4). (d) shows the detector responses from relaxation data measured at these three fields and also shows the fitted exchange contribution (plotted value corresponds to 600 MHz, where $R_{2,ex} \propto B_0^2$). Error bars indicate the 95% confidence interval, determined by Monte Carlo error analysis (200 repetitions).[13] Each plot in (b) and (d) indicates z_0 and Δz, which are the center of the detector and the effective width of the detector, which approximate the average correlation time and the range of correlation times a detector is sensitive to (both on log-scales, with precise definitions given in the supplementary material, glossary). Data fits are found in supplementary material, Figs. S7 and S9.

fully remove all relaxation contributions due to overall tumbling or may remove too much, depending on bond orientation. This difference in the relaxation could be wrongly interpreted as internal dynamics. A treatment that substitutes the overall correlation function in Eq. (13) with a correlation function for anisotropic tumbling would improve the analysis, especially for molecules with larger anisotropies of the rotational diffusion tensor. We are currently implementing such a scheme, which is beyond the scope of the present paper.

We have investigated whether our results were significantly biased by this simplification. The amount of relaxation due to tumbling depends directly on the orientation of the individual H–N bond vectors relative to the diffusion tensor (strictly speaking the orientation of the H–N dipole coupling and ^{15}N CSA tensors, which are not exactly aligned). For example, R_2 relaxation due to tumbling should be faster where the bond vectors point along the z-axis since rotational diffusion of the z-axis is slower. Therefore, we plot the square of the z-component of the bond vector in the PAS of the diffusion tensor (the bond vector is normalized to a length of 1, and the square is relevant for relaxation). Results are shown in Fig. 9; there appears to be some correlation so that when $[\nu_{HN}]_z^2$ becomes small, $\rho_4^{(\theta,S)}$ increases (residues 18–20, 35–36, especially 51–54, 63). This is somewhat expected as, for H–N bond vectors perpendicular to the z-axis of the PAS, tumbling motion is slightly faster than the overall correlation time, inducing faster R_1 relaxation; this additional relaxation is underestimated in the correction by the term R_ζ^0, and then, the increased relaxation rate increases $\rho_4^{(\theta,S)}$. Although the effect is weak, it will be necessary to improve the

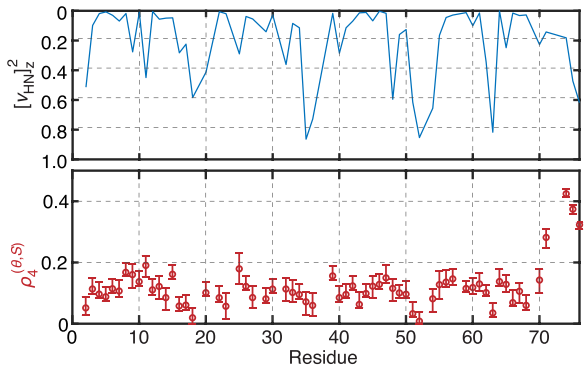

FIG. 9. Square of the component of the H–N bond vectors parallel with the z-component of the diffusion tensor. There is weak correlation between increases in $[\nu_{HN}]_z^2$ and decreases in $\rho_4^{(\theta,S)}$, as seen in the comparison here ($[\nu_{HN}]_z^2$ is plotted with an inverted axis for better comparison). $\rho_4^{(\theta,S)}$ values are the same as those shown in Fig. 8(d).

diffusional model for systems with larger anisotropies to avoid significant distortions.

A. Comparison to model-free analysis

The detector analyses (Fig. 8) may be compared to a model-free/extended model-free analysis of relaxation data sets recorded at three magnetic fields, which is shown in Fig. 10. The model-free analysis was performed by Charlier *et al.*,[31] using the program DYNAMICS.[39] Model-free analysis displays some discontinuity of the fitted parameters along the primary sequence. Discontinuity appears to have two primary sources. The first is model selection: relaxation data are analyzed in this example with four different models of the correlation function. One uses either one or two motions in the model, and in some cases, it is assumed that the correlation time of the faster motion is too short to directly induce relaxation so that only its amplitude is fitted. Then, models with anywhere from one to four parameters are applied ($[S_f^2]$, $[S_f^2, \tau_f]$, $[S_s^2, \tau_s, S_f^2]$, or $[S_s^2, \tau_s, S_f^2, \tau_f]$). Typically, if the model applied varies from one residue to the next, it is accompanied by significant jumps in the model parameters. For example, the $\beta1$-$\beta2$ turn (residues 7–13) exhibits more motion than surrounding residues. We would expect this motion to be partly correlated among these residues so that the correlation times should be similar. Yet, between residues 9, 10, and 11, τ_s varies by about half an order of magnitude, with noticeable variation for the other residues as well (where no strong variation appears in the raw data, Fig. S9). Indeed,

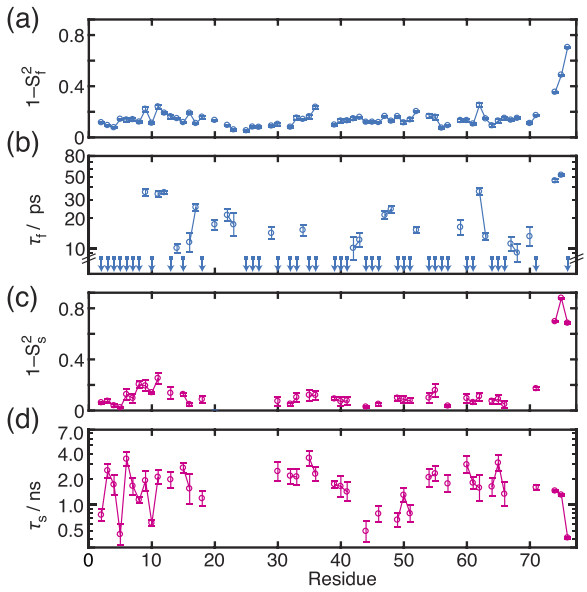

FIG. 10. Model-free analysis of ubiquitin high-field data as previously reported by Charlier *et al.*,[31] using the same data as in Fig. 8(b). (a) shows $(1 - S_f^2)$ for the fast motion. (b) plots τ_f, the correlation time of the fast motion. In some cases, S_f^2 is fitted but τ_f is not, where it is assumed τ_f is too short to induce relaxation, as indicated with a downward pointing arrow (below 10 ps on the y-axis). (c) and (d) plot slow motion, showing $(1 - S_s^2)$ and τ_s, respectively. In some cases, only one motion was fitted, which is then displayed as a fast motion.

three different models were employed to analyze relaxation for $\beta1$-$\beta2$ turn: a simple model-free model for residue 12, an extended model-free model with no correlation time for fast motion (too fast to be determined) for residues 7, 8, 10, and 13, and a full extended model-free with two defined correlation times for residues 9 and 11.

The interpretation of these jumps in models and parameters is not trivial: they might be due to real differences in local motions or, perhaps more likely, to small fluctuations of the measured rates or experimental noise that skews the model selection, one way or another. It is thus difficult to interpret all correlation times as true correlation times, and it is safer to consider these as effective correlation times, potentially representing multiple motions or motions defined by multiple correlation times. Model selection is considered a necessary evil in order to make the most of the information content of relaxation data sets. Alternatives to model selection have been suggested, where a model-free approach[40] or a different model[4,5] is used consistently to analyze an entire relaxation data set. By contrast, detectors can be applied without model selection between residues, and when dynamics may be explained simply (fewer parameters), some of the detector responses simply approach zero, without requiring a new model, significantly reducing discontinuity in the resulting parameters.

Variation in model-free analysis parameters may also occur without model selection. The longest stretch of residues analyzed using a single model occurs on residues 2–8 (3 parameters). Significant variation occurs for τ_s, sometimes exceeding an order of magnitude between neighboring residues, and this variation is accompanied by smaller jumps in $(1 - S_s^2)$, with longer correlation times correlated with larger values of $(1 - S_s^2)$. The strongest outliers for τ_s are found at residues 2 and 5, where differences are driven by sharp reduction in R_1 at these residues (Fig. S9), which can be explained by less motion at long correlation times or more motion at short correlation times [see Figs. 5(b) and 5(d)]. In the model-free analysis, the changes in R_1 are explained as a decrease in τ_s and a decrease in $(1 - S_s^2)$.

The following question arises: is there really a motion at residues 2 and 5 with a shorter correlation time ($\sim 10^{-9.2}$ s = 630 ps) that is absent at the surrounding residues? The detector analysis suggests that this does not need to be the case: $\rho_3^{(\theta,S)}$ is particularly sensitive to this range of correlation times and shows almost no change in detector response. Instead, it explains the decrease in R_1 at residue 2 as a decrease in motion at longer correlation times ($\rho_4^{(\theta,S)}$), and the decrease in R_1 at residue 5 as an increase in motion at short correlation times ($\rho_1^{(\theta,S)}$). Differences in responses of the two residues results from differences in the experimental R_2 data (Fig. S9). Note that this does not *disprove* the results of model-free analysis: it is possible that the simultaneously decreasing values of τ_s and $(1 - S_s^2)$ cancel each other out, resulting in the apparent uniformity of $\rho_3^{(\theta,S)}$ (model-free and detector analyses should usually be consistent, but detectors can be more broadly interpreted[13]). However, just as model selection requires us to consider that the fitted correlation times may be effective correlation times, even if only a single model is applied, we must still consider that the resulting parameters are effective and represent multiple motions (see

Fig. 2). When this is the case, detectors give a more direct picture of the distributions of motion that lead to the effective model parameters.

The limitations of the use of a single effective correlation time were discussed in the original article by Lipari and Szabo.[9] In particular, Lipari and Szabo showed that drastically different distributions of correlation times can lead to very similar observables (see Fig. 3 of Ref. 9), particularly when the spectral density function is only probed at a handful of frequencies. Thus, one should keep in mind that correlation times in the model-free approach are effective. By contrast, the detector analysis provides information about the amplitude of motion over a given range of frequencies and has a well-defined relationship to the distribution of motion [Eq. (20)]. This information is less model-dependent and less prone to overinterpretation. In addition, the use of a single model to analyze relaxation rate constants for the entire protein makes direct comparison between given residues easier and facilitates the interpretation of variations of detector responses.

B. Relationship to the LeMaster approach

The limits of conventional model-free analysis have motivated development of the dynamic detector method of analysis and its subsequent adaptation for solution-state dynamics. Other alternative methods have been proposed to analyze relaxation data sets. For example, the spectral-density mapping method[14–16] of analyzing relaxation data acquired at one or several magnetic fields (R_1, R_2, σ_{NH} rate constants) avoids distortion of dynamic information. It turns out that spectral density mapping is a special case of dynamics detectors (as previously discussed, see Ref. 13 Sec. III D). However, spectral-density mapping only yields the spectral densities at a few frequencies. Thus, it does not provide directly quantitative information about correlation times. In addition, spectral-density mapping describes the total motion including tumbling, forgoing the separation of internal motion and tumbling motion. LeMaster addressed this limitation[21] by introducing an alternative analysis of solution-state relaxation data, acquired at a single field, which accounts for tumbling. In his approach, he suggested fitting the three relaxation rate constants to a spectral density of the following form:

$$J(\omega_i) = \frac{2}{5} S_f^2 \left[S_H^2 S_N^2 \frac{\tau_r}{1+(\omega_i \tau_r)^2} + (1 - S_H^2) \frac{\tau_H}{1+(\omega_i \tau_H)^2} + S_H^2 (1 - S_N^2) \frac{\tau_N}{1+(\omega_i \tau_N)^2} \right]. \quad (27)$$

Rather than having five free parameters for each residue (S_f^2, S_H^2, S_N^2, τ_H, τ_N, where τ_r is determined from the complete data set of all residues), LeMaster proposed fixing $\tau_H = 1/(\omega_H + \omega_N)$ and $\tau_N = -1/\omega_N$ so that $(1 - S_f^2)$ is the amplitude of motion for short correlation times, $(1 - S_H^2)$ characterizes motion for correlation times nearest to τ_H, and $(1 - S_N^2)$ characterizes motion for correlation times nearest to τ_N. This model accounts explicitly for the bias in the frequencies at which the spectral density is probed by relaxation.

If we rearrange the spectral density as follows

$$\begin{aligned} S_f^2 S_H^2 S_N^2 &= 1 - (1 - S_f^2 S_H^2 S_N^2) \\ &= 1 - \left(1 - S_f^2 + S_f^2 (1 - S_H^2) + S_f^2 S_H^2 (1 - S_N^2)\right) \\ J(\omega_i) = \frac{2}{5} \Bigg[& \frac{\tau_r}{1+(\omega_i \tau_r)^2} + (1 - S_f^2) \frac{-\tau_r}{1+(\omega_i \tau_r)^2} \\ & + S_f^2 (1 - S_H^2) \left(\frac{\tau_H}{1+(\omega_i \tau_H)^2} - \frac{\tau_r}{1+(\omega_i \tau_r)^2} \right) \\ & + S_f^2 S_H^2 (1 - S_N^2) \left(\frac{\tau_N}{1+(\omega_i \tau_N)^2} - \frac{\tau_r}{1+(\omega_i \tau_r)^2} \right) \Bigg], \end{aligned} \quad (28)$$

we see that the spectral density is a linear function of $(1 - S_f^2)$, $S_f^2(1-S_H^2)$, and $S_f^2 S_H^2(1-S_N^2)$, with a fixed offset term. In fact, the coefficients of these three terms include a negative contribution due to internal motion attenuating relaxation from tumbling. This is similar to the design of sensitivities to internal motion [$R_\zeta^{solu.}(z_i)$] in the detector analysis [Eq. (18)].

We have derived the sensitivity of these three terms as a function of correlation time and compared them to the detector sensitivities (Fig. 11). Detector sensitivities and amplitudes of the terms in LeMaster's approach [Eq. (28)] are remarkably similar to the detector sensitivities for the same data set. Furthermore, the correlation times for the maximum sensitivities of ρ_2 and ρ_3, and $S_f^2(1 - S_H^2)$ and $S_f^2 S_H^2(1 - S_N^2)$, nearly coincide with τ_H and τ_N, the fixed correlation times used by LeMaster. When comparing to detector sensitivity, one notes that the amplitudes using LeMaster's approach become slightly more negative for some correlation times, which may lead to small differences as compared to the detector approach. LeMaster's approach is a special case of the more general detector approach for relaxation data sets recorded at a single magnetic field.

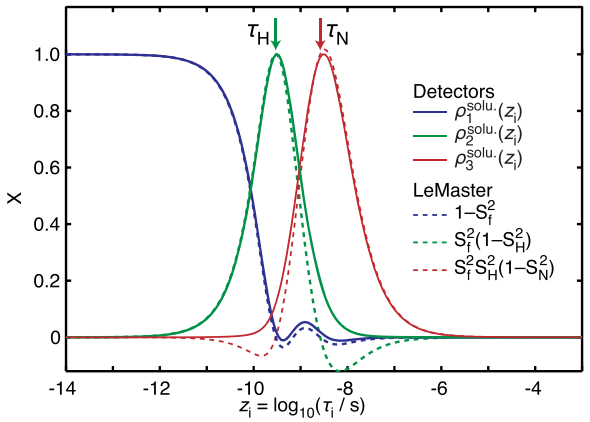

FIG. 11. Detectors vs LeMaster approach. Solid lines show three detector sensitivities optimized from R_1, R_2, and σ_{NH} rate constants at 600 MHz, assuming a rotational correlation time of 4.84 ns. Dashed lines show the sensitivities of the three terms resulting from the LeMaster approach. Arrows indicate the position of τ_H and τ_N. One sees that the resulting behavior is very similar, although the LeMaster approach results in more regions of negative sensitivity.

IV. CONCLUSIONS

Dynamics detectors have been developed to characterize distributions of motion of arbitrary complexity using solution-state NMR relaxation data. A set of detectors is optimized for a given experimental relaxation data set, where each detector characterizes the amount of motion for a well-defined range of correlation times. The approach is an adaptation of the concept developed for solid-state NMR relaxation data. We obtain detectors that are sensitive to the internal motion of a molecule tumbling in solution but are not sensitive to the tumbling motion itself. This is accomplished by defining rate-constant sensitivities to the internal motion for molecules tumbling isotropically in solution and obtaining detectors from these sensitivities. Detector analysis does not suffer from the biases of model-free/extended model-free analyses of relaxation data: when using model-free formalism to analyze relaxation data with an underlying complex distribution of motion, the results are difficult to interpret in terms of the physical motion. We apply the detector method to the analysis of ^{15}N relaxation rate constants in ubiquitin and find a more easily interpretable and stable description of internal dynamics than is obtained with conventional model-free analysis. This demonstrates the utility of the detector approach in solution-state NMR.

SUPPLEMENTARY MATERIAL

See supplementary material attached to this manuscript that contains a glossary of new terminology for detector analysis, a detailed explanation of detector design using singular value decomposition, an investigation into model selection criteria (number of detectors), analysis of a two-field data set, plots of the experimental data fits, and tables of detection vectors used for fitting.

ACKNOWLEDGMENTS

This work was supported by the Swiss National Science Foundation (Grant Nos. 200020_159707 and 200020_178792). This project has also received funding from the European Research Council (ERC) under the European Union's Horizon 2020 research and innovation program (Grant Agreement No. 741863, FASTER) and under the European Union's Seventh Framework Programme (FP7/2007–2013), ERC Grant Agreement No. 279519 (2F4BIODYN) (to F.F.).

REFERENCES

[1] A. G. I. Palmer, Chem. Rev. **104**(8), 3623 (2004).
[2] C. Charlier, S. F. Cousin, and F. Ferrage, Chem. Soc. Rev. **45**(9), 2410 (2016).
[3] J. R. Brainard and A. Szabo, Biochemistry **20**(16), 4618 (1981).
[4] V. Calandrini, D. Abergel, and G. R. Kneller, J. Chem. Phys. **133**(14), 145101 (2010).
[5] V. Tugarinov, Z. Liang, Y. E. Shapiro, J. H. Freed, and E. Meirovitch, J. Am. Chem. Soc. **123**(13), 3055 (2001).
[6] G. M. Clore, A. Szabo, A. Bax, L. E. Kay, P. C. Driscoll, and A. M. Gronenborn, J. Am. Chem. Soc. **112**, 4989 (1990).
[7] B. Halle, J. Chem. Phys. **131**, 224507 (2009).
[8] L. E. Kay, D. A. Torchia, and A. Bax, Biochemistry **28**(23), 8972 (2002).
[9] G. Lipari and A. Szabo, J. Am. Chem. Soc. **104**(17), 4546 (1982).
[10] A. Abragam, *The Principles of Nuclear Magnetism* (Clarendon Press, Oxford, 1961).
[11] M. P. Nicholas, E. Eryilmaz, F. Ferrage, D. Cowburn, and R. Ghose, Prog. Nucl. Magn. Reson. Spectrosc. **57**(2), 111 (2010).
[12] A. A. Smith, M. Ernst, and B. H. Meier, Angew. Chem., Int. Ed. **56**(44), 13590 (2017).
[13] A. A. Smith, M. Ernst, and B. H. Meier, J. Chem. Phys. **148**(4), 045104 (2018).
[14] N. A. Farrow, O. Zhang, A. Szabo, D. A. Torchia, and L. E. Kay, J. Biomol. NMR **6**(2), 153 (1995).
[15] R. Ishima and K. Nagayama, J. Magn. Res., Ser. B **108**(1), 73 (1995).
[16] J. Peng and G. Wagner, J. Magn. Reson. **98**(2), 308 (1992).
[17] P. Kaderavek, V. Zapletal, R. Fiala, P. Srb, P. Padrta, J. P. Precechtelova, M. Soltesova, J. Kowalewski, G. Widmalm, J. Chmelik, V. Sklenar, and L. Zidek, J. Magn. Reson. **266**, 23 (2016).
[18] A. Hsu, P. A. O'Brien, S. Bhattacharya, M. Rance, and A. G. Palmer III, Methods **138-139**, 76 (2018).
[19] J. F. Lefevre, K. T. Dayie, J. W. Peng, and G. Wagner, Biochemistry **35**(8), 2674 (1996).
[20] S. N. Khan, C. Charlier, R. Augustyniak, N. Salvi, V. Dejean, G. Bodenhausen, O. Lequin, P. Pelupessy, and F. Ferrage, Biophys. J. **109**(5), 988 (2015).
[21] D. M. LeMaster, J. Biomol. NMR **6**(4), 366 (1995).
[22] A. Hsu, F. Ferrage, and A. G. Palmer III, Biophys. J. **115**(12), 2301 (2018).
[23] A. A. Smith, M. Ernst, S. Riniker, and B. H. Meier, Angew. Chem., Int. Ed. **58**, 9383 (2019).
[24] A. A. Smith, M. Ernst, and B. H. Meier, Distortion Free Relaxation Analysis Technique software, URL: http://difrate.sourceforge.net, 2018.
[25] B. Halle and H. Wennerström, J. Chem. Phys. **75**(4), 1928 (1981).
[26] P. Ma, Y. Xue, N. Coquelle, J. D. Haller, T. Yuwen, I. Ayala, O. Mikhailovskii, D. Willbold, J.-P. Colletier, N. R. Skrynnikov, and P. Schanda, Nat. Commun. **6**, 8361 (2015).
[27] A. Krushelnitsky, D. Gauto, D. C. Rodriguez Camargo, P. Schanda, and K. Saalwachter, J. Biomol. NMR **71**(1), 53 (2018).
[28] A. A. Smith, E. Testori, R. Cadalbert, B. H. Meier, and M. Ernst, J. Biomol. NMR **65**(3-4), 171 (2016).
[29] O. Walker, R. Varadan, and D. Fushman, J. Magn. Reson. **168**(2), 336 (2004).
[30] G. Golub and W. Kahan, J. Soc. Ind. Appl. Math. Ser. B. Num. Anal. **2**(2), 205 (1965).
[31] C. Charlier, S. N. Khan, T. Marquardsen, P. Pelupessy, V. Reiss, D. Sakellariou, G. Bodenhausen, F. Engelke, and F. Ferrage, J. Am. Chem. Soc. **135**(49), 18665 (2013).
[32] H. Akaike, IEEE Trans. Autom. Control **19**(6), 716 (1974).
[33] F. Bayer and F. Cribari-Neto, TEST **24**(4), 776 (2015); e-print arXiv:1405.4525 [stat.CO].
[34] J. Shang and J. Cavanaugh, Comput. Stat. Data. Anal. **52**(4), 2004 (2008).
[35] C. M. Hurvich and C.-L. Tsai, J. Time Ser. Anal. **14**(3), 271 (1993).
[36] N. Sugiura, Commun. Stat.: Theory Methods **7**, 13 (1978).
[37] F. Massi, M. J. Grey, and A. G. Palmer III, Protein Sci. **14**(3), 735 (2005).
[38] D. F. Hansen, H. Feng, Z. Zhou, Y. Bai, and L. E. Kay, J. Am. Chem. Soc. **131**(44), 16257 (2009).
[39] D. Fushman, Methods Mol. Biol. **831**, 485 (2012).
[40] S. F. Cousin, P. Kaderavek, N. Bolik-Coulon, Y. Gu, C. Charlier, L. Carlier, L. Bruschweiler-Li, T. Marquardsen, J. M. Tyburn, R. Bruschweiler, and F. Ferrage, J. Am. Chem. Soc. **140**(41), 13456 (2018).